

Predicting the Voltage Dependence of Interfacial Electrochemical Processes at Lithium-Intercalated Graphite Edge Planes

Kevin Leung

Sandia National Laboratories, MS 1415,

Albuquerque, NM 87185

kleung@sandia.gov (505)8441588

(Dated: February 5, 2021)

Abstract

The applied potential governs lithium-intercalation and electrode passivation reactions in lithium ion batteries, but are challenging to calibrate in condensed phase DFT calculations. In this work, the “anode potential” of charge-neutral lithium-intercalated graphite (LiC_6) with oxidized edge planes is computed as a function of Li-content (n_{Li}) at edge planes, using *ab initio* molecular dynamics (AIMD), a previously introduced Li^+ transfer free energy method, and the experimental $\text{Li}^+/\text{Li(s)}$ value as reference. The voltage assignments are corroborated using explicit electron transfer from fluoroethylene carbonate radical anion markers. PF_6^- is shown to decompose electrochemically (i.e., not just thermally) at low potentials imposed by our voltage calibration technique. We demonstrate that excess electrons reside in localized states-in-the-gap in the organic carbonate liquid region, which is not semiconductor-like (band-state-like) as widely assumed in the literature.

keywords: lithium ion batteries; voltage prediction; density functional theory; *ab initio* molecule dynamics; computational electrochemistry

I. INTRODUCTION

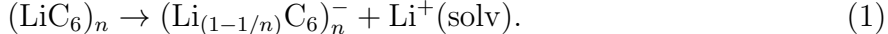
The applied potential governs the thermodynamics and kinetics of lithium ion battery (LIB) interfacial processes. Li^+ insertion into graphite anodes to form LiC_6 is completed at 0.1 V vs. $\text{Li}^+/\text{Li(s)}$, or ~ -2.9 V vs. standard hydrogen potential. Before this low voltage is reached, commonly used battery electrolytes containing ethylene carbonate (EC), cosolvents, and $\text{Li}^+/\text{PF}_6^-$ salt already decompose at 0.7-0.8 V vs. $\text{Li}^+/\text{Li(s)}$. Fortunately, the growth of self-limiting films (called “solid-electrolyte interphase,” or SEI) formed via electron-injection-induced sacrificial electrolyte degradation passivates and stabilizes the anode.^{1,2} SEI considerations are also relevant for new anode materials like silicon. To interpret measurements and to help devise better artificial SEI/passivation layers,³ there is a need to use electronic structure computational tools (e.g., Density Functional Theory, DFT) to predict the voltage dependence of liquid-solid interfacial processes. Such a capability will have significant impact for studying not just LIB,^{4,5} but also lithium-air batteries,⁶ water-splitting processes,^{7,8} and broad areas relevant to fuel cells, catalysis,⁹⁻¹² and electrodeposition.^{13,14} In this work, we validate a recently devised potential calibration scheme,¹⁵ apply it to interfaces between liquid EC and oxidized edge planes of LiC_6 , and explore the possibility of electrochemical decomposition of the counter-ion (PF_6^-) used in commercial LIB electrolytes. In the electronic supporting information (S.I.), we document the significant error that can arise if the liquid electrolyte is omitted in voltage estimates at interfaces.

For non-redox active systems like non-Faradaic supercapacitors, the voltage difference between two electrodes arises from their different surface charges mediated by electric double layers in the liquid region.¹⁶ In contrast, on complex LIB electrode surfaces, what a certain “applied voltage” means at the atomic level has not been sufficiently conceptualized, partly due to the difficulty in probing details at such lengthscales.¹⁷ On the theory side, potential calibration has been challenging in periodic boundary conditions, condensed-phase DFT simulations that depict liquid-solid interfaces.⁸⁻¹² DFT calculations are performed at constant number of electrons, not constant voltage. Each DFT simulation cell is associated with one electrode/Fermi level and is incompatible with a second reference electrode. Furthermore, most DFT electrochemistry calculations are conducted at $T=0$ K, which precludes explicit treatment of liquid solvents, dissolved salts, and, in the majority of cases, charged interfaces. Several interesting recent advances have coupled the Poisson-Boltzmann equation or related

approaches to DFT at the expense of introducing vacuum-solid or -liquid interfaces into the model.^{9,10} (The vacuum layer in effect serves as the reference electrode.) Purely condensed phase simulations with no vacuum region require other methods.

We recently estimated what will be called the “anode potential” (\mathcal{V}) of inert LiC_6 basal planes at finite temperature.¹⁵ The justification is briefly and heuristically described here. Our approach seeks to mimic LIB experimental processes, where Li-deintercalation occurs via transfer of Li^+ from LiC_6 , through the liquid-solid interface, to the liquid electrolyte, and ultimately into the Li metal counter electrode not explicitly depicted in the simulation. e^- flows in the same direction, but through the external circuit. Experimentally, it is known that these charge transfer processes occur at the onset potential of 0.1 V vs. $\text{Li}^+/\text{Li}(\text{s})$.

We model this half-cell reaction at the onset of LiC_6 delithiation,



While our model does not include counter electrodes, and the excess e^- is left on the anode in the simulation (with finite surface area correction, see below), Eq. 1 has effectively completed the e^- circuit. This is because, at equilibrium and in the absence of load-induced voltage drop, the Fermi level (E_F) of the Li metal “counter electrode” in our thought experiment must be lowered by 0.1 V to coincide with the E_F of LiC_6 . Under these conditions, the excess e^- on $\text{Li}_{1-\delta}\text{C}_6$ can start to flow to $\text{Li}(\text{s})$. By reaching equilibrium (tuning the free energy change (ΔG_t) of the Eq. 1 to zero) via varying the surface charge (σ) on the electrode surface, we arrive at the experimentally known half-cell voltage for this reaction. This is the reference point that can be pegged to measurements. Away from this $\mathcal{V}=0.1$ V vs. $\text{Li}^+/\text{Li}(\text{s})$ fixed point, anode voltages are clearly related to the free energy of monovalent Li^+ transfer between LiC_6 and EC liquid (ΔG_t), $\Delta \mathcal{V} = -\Delta G_t/|e|$, provided that the interior Li atoms are frozen and not allowed to leak into the electrolyte (i.e., there is no redox reaction), which is the case in our simulations.¹⁵ The σ - \mathcal{V} relationship associated with our frozen-Li basal plane LiC_6 model electrode is reminiscent of those in non-Faradaic supercapacitors.

The *ab initio* molecular dynamics (AIMD, or DFT/MD) technique is used to calculate ΔG_t .¹⁵ ΔG_t calculations deal with physical ions, not infinitesimal/theoretical test charges, and therefore circumvent formal/unmeasurable concepts like the difference between “Volta” and “Galvani” definitions of the potential.^{8,18} Further justification, including a thought experiment on explicitly including the interface between the liquid electrolyte and the Li

metal reference electrode, and comparison between our approach and related methods found in the aqueous computational electrochemistry literature, are given in Ref. 15.

The present work focuses on LiC_6 edge planes through which Li^+ can intercalate and deintercalate. Edge planes are far more technologically relevant and complex than the proof-of-principle pristine basal plane considered previously.¹⁵ But the same theoretical method can be used to examine the edge plane voltage. Indeed, Ref. 15 (Fig. 2) implies that this Li^+ transfer protocol can in principle directly compare the voltage on any two electrodes. This is because a sufficiently thick liquid electrolyte region intervening between a basal and an edge plane can chemically and electrostatically screen them from each other. So the difference in equilibrium free energies of Li^+ transfer from each electrodes to the electrolyte, divided by $|e|$ should be proportional to their voltage difference. Since LiC_6 is an electronic conductor, at equilibrium e^- flows between surfaces to make the voltage the same on basal and edge planes. On pristine edge planes, the all-important $\Delta G_t=0$ point is determined not only by the electronic charge (σ) compensated by mobile Li^+ in the liquid electrolyte, but also the fraction of Li occupying the edge sites (n_{Li}). At a fixed, applied potential, these two quantities should adjust themselves to minimize the free energy of the system. For the illustrative purpose of this work, we have fixed $\sigma=0$ and only varied n_{Li} , and \mathcal{V} can be considered the instantaneous voltage before the edge Li^+ content can change.

Our predicted edge plane voltage as n_{Li} varies will be corroborated using explicit electron transfer from fluoroethylene carbonate radical anion markers. Using AIMD simulations with appropriately calibrated potentials, PF_6^- is shown to exhibit concerted e^- transfer and bond-breaking reactions at low voltages, suggesting that under such conditions electrochemical decomposition may need to be considered. This is significant because it is widely accepted that PF_6^- decomposes only thermally or due to reaction with trace water.^{19,20} Finally, the simulation cells used in this work provide information about the electronic orbital alignment at explicit electrode/electrolyte interfaces. We show that excess electrons reside in localized states-in-the-gap in the organic carbonate liquid region, not in delocalized states at the conduction band minimum. The band structure is *not* semiconductor-like (band-state-like) as widely assumed in the literature.²¹

	n_{Li}	$N(\text{Li})$	λ	t_{max}	$\langle dH(\lambda)/d\lambda \rangle_{\lambda}$	ΔG_t
A	0.417	0	0.211	43.9	+5.45±0.11	
B	0.417	0	0.789	44.4	-6.63±0.04	-1.14
C	0.500	0	0.211	52.1	+5.86±0.10	
D	0.500	0	0.789	40.8	-6.31±0.10	-0.78
E	0.583	0	0.211	26.1	+6.59±0.11	
F	0.583	0	0.789	20.9	-6.23±0.11	-0.36
G	0.417	1	0.211	25.0	+5.80±0.05	
H	0.417	1	0.789	25.2	-6.61±0.07	-0.94

TABLE I: Details of AIMD trajectories for ΔG_t calculations. $N(\text{Li})$ is the number of mobile Li^+ in the liquid region, and λ is the net charge of the $\text{Li}^{\lambda+}$ ion frozen in the middle of the liquid. t_{max} is the total trajectory duration in picoseconds, and include the first 1 ps equilibration discarded when collecting statistics. The exceptions are C & D, where t_{max} includes the discarded first 10 ps. Integrands and ΔG_t are in eV; the latter is obtained by averaging the two integrands, and includes a -0.39 eV entropic correction and a -0.15 eV correction for using a 2-point treatment of Li^+ solvation.¹⁵ To convert $(-\Delta G_t)$ to \mathcal{V} , add 0.1 V for $\text{Li}^+/\text{Li}(\text{s})$ and 0.1 V for the “half e^- rule” (see text).

II. METHOD

Our simplified electrode model consists of a LiC_6 strip with all C=O termination.^{22,23} Four neighboring C=O bonds form a pocket where Li^+ can reside. The Li^+ surface density (n_{Li}) is unity if all such pockets are occupied. Figure 1 depicts the periodically replicated $29.74 \times 14.97 \times 15.06 \text{ \AA}^3$ interfacial simulation cell containing a $\text{Li}_x\text{C}_{192}\text{O}_{48}$ anode slab and 32 EC molecules. Interior atoms in the anode, with LiC_6 stoichiometry, are frozen while C, O, and Li atoms at the edges are allowed to move. $n_{\text{Li}} < 1$ electrode configurations are obtained by randomly, and as uniformly as possible, removing Li atoms from the two LiC_6 edge planes.

AIMD trajectories and a two-point thermodynamic integration (T.I.) formula with corrections/extrapolations are used to compute ΔG_t (Table I). These simulations apply the VASP code²⁴ with PAW pseudopotentials²⁵ and the DFT/PBE functional.²⁶ An energy cut-off of

400 eV, 10^{-6} eV wavefunction convergence, and Γ -point sampling are enforced. Spot checks show that $1 \times 2 \times 2$ k -point sampling changes the integrands in ΔG_t by less than ~ 0.05 eV, similar to basal plane cases.¹⁵ A thermostat keeps the trajectories at an elevated $T=450$ K to improve statistics and prevent EC crystallization. Tritium masses are substituted for proton masses to permit 1 fs time steps. Compared to the previous work,¹⁵ the predicted ΔG_t is shifted by -0.17 V to correct the prior neglect of quantum nuclear effect inside bulk LiC_6 and the inadvertent use of $T=450$ K when adding translational and vibrational entropies to compare with experiments performed at $T=300$ K.

The trajectories are initiated using Monte Carlo (MC) simulations in which anode atoms are frozen in DFT/PBE-optimized configurations. LIB salt concentration is typically 1.0 M, the static dielectric constant is large (Debye length ~ 3 Å), and electrode surfaces should be screened from each other even in a small simulation cell. Electrical double layers should be well-equilibrated to the extent that the simple classical force fields used are accurate. More MC details are described in the S.I.

III. RESULTS

A. Controlling Potential at LiC_6 Edge Planes

Instead of mapping the entire two-dimensional potential $\mathcal{V}(n_{\text{Li}}, \sigma)$, we focus on $\sigma = 0$. In Fig. 1a, the linearly extrapolated $\mathcal{V}(\sigma = 0, n_{\text{Li}})$ reaches the LiC_6 experimental plateau voltage of 0.1 V vs. $\text{Li}^+/\text{Li}(\text{s})$ at $n_{\text{Li}} \sim 0.69$. If $n_{\text{Li}} > 0.69$, $\sigma > 0$ would be needed to raise $\mathcal{V}(\sigma, n_{\text{Li}})$ back to the green line and achieve the experimental potential associated with LiC_6 . This merely means that some of the edge Li must then be considered Li^+ ions — not atoms — compensated with mobile PF_6^- further away in the electrolyte.²⁷

Note that a “half-electron rule” vertical shift has been included to convert ΔG_t (Table I) to $\mathcal{V}(\sigma = 0, n_{\text{Li}})$ (Fig. 1a). T.I. calculations involve moving a Li^+ from LiC_6 to the middle of the solvent region of a charge-neutral simulation cell, leaving an e^- behind. Along the T.I. path, an average of half an e^- , or $\sigma = -|e|/(4A)$, exists on the two electrode surfaces, where A is the lateral surface area. We assume this excess charge is uniformly distributed on the conducting electrode surfaces, in accordance with classical electrostatic predictions; see the S.I. of Ref. 15 for analysis of instantaneous charge distributions. The effect of this

average σ is estimated by finite difference and subtracted from Fig. 1a, as follows. We inject one mobile Li^+ , compensating an excess e^- on the electrode, and recompute ΔG_t (Table I, trajectories G-H). The simulation cells remain charge-neutral. $\Delta\mathcal{V}$ is found to be -0.20 V ($\delta\sigma/\delta\mathcal{V}=17.8 \mu\text{C}/(\text{cm}^2\text{V})$) after adding the one e^- . This is smaller in magnitude than that in basal plane simulation cells.¹⁵ To undo this surface charging effect, a $+0.1$ V correction is thus applied. The shift vanishes at large A , and represents an extrapolation to infinite system size. We stress that experimentalists can impose a potential without knowing details about the surfaces, but DFT calculations work differently; σ and n_{Li} need to be adjusted to arrive at the desired voltage.

In the absence of the liquid electrolyte, the potential at zero surface charge is directly related to the work function of the electrode in vacuum. In the S.I., we report work functions and show that the potential in vacuum, predicted as a function of n_{Li} , is significantly modified by the inclusion of the liquid electrolyte in the main text. This observation dovetails with predictions that work functions of metals can vary by ~ 1 V when their surfaces are covered with a monolayer of water¹² or organic molecules.²⁸

Although linear extrapolation is not expected to hold over the entire n_{Li} range, $\mathcal{V}(n_{\text{Li}}, \sigma = 0)$ appears to extrapolate to a value substantially below 0 V vs. $\text{Li}^+/\text{Li}(\text{s})$ at $n_{\text{Li}}=1$. Negative potentials relative to $\text{Li}^+/\text{Li}(\text{s})$ are below the operating conditions of LIB anodes. This strongly suggests that $\sigma=0$ and $n_{\text{Li}}=1$ yield an overpotential for electrolyte decomposition. In the literature, C=O edge AIMD simulations have been reported at $n_{\text{Li}}=1$ and $\sigma=0$, and EC molecules are found to decompose in picosecond via two different $2-e^-$ mechanisms, releasing CO and C_2H_4 gases, respectively.²² What are the potential dependences of these two competing processes? Recently, it has been predicted that the $2-e^-$ CO-releasing route has a far lower reaction barrier than C_2H_4 generation in bulk liquid electrolyte regions.²⁹ It is therefore unlikely that C_2H_4 should be a dominant $2-e^-$ product unless there is an overpotential. Consistent with this deduction, Fig. 1 indeed suggests the Ref. 22 system, where $n_{\text{Li}} = 1$, is at $\mathcal{V} < 0$ V. If this were not the case, mostly CO products are expected. Note that two-electron reduction can yield C_2H_4 gas if e^- are added sequentially, not simultaneously, separated by milliseconds.²⁹ This timescale is far larger than our AIMD trajectory durations.

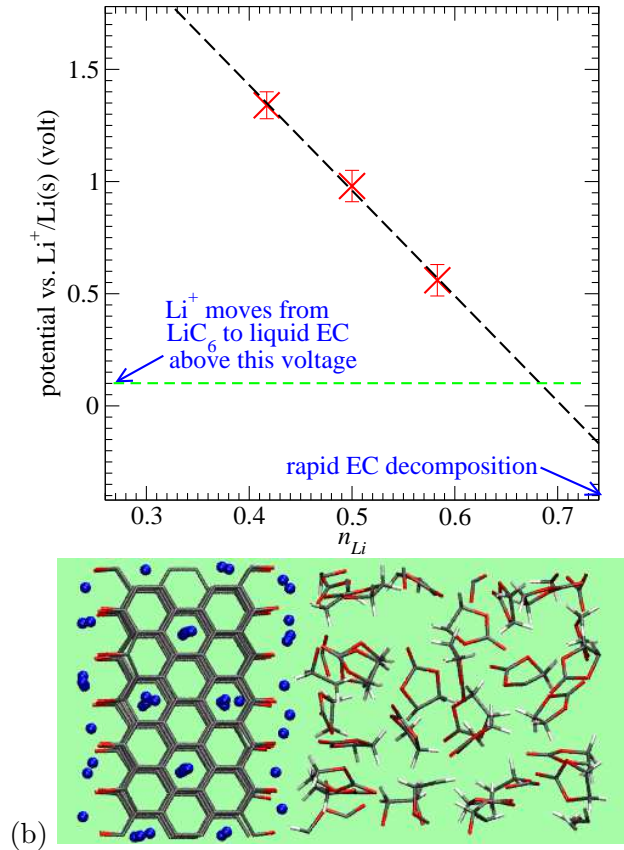


FIG. 1: (a) \mathcal{V} at zero electronic charge as a function of edge plane Li content. The dashed line is a linear extrapolation. (b) A snapshot of the edge plane interfacial simulation cell. C, O, H, and Li are grey, red, white, and blue, respectively.

B. Validating Predicted Potential: Electron Transfer

The predicted potential should not depend on whether Li^+ or e^- moves across the interface. Next we demonstrate that $\mathcal{V}(\sigma = 0, n_{\text{Li}})$, calibrated using Li^+ transfer above, is also consistent with e^- transfer. In the middle of the liquid region is placed a fluoroethylene carbonate (FEC^-) radical anion (Fig. 2), which is an effective electrolyte additive molecule for improving SEI on anode surfaces.³⁰ In charge-neutral FEC (Fig. 2c), the carbonyl carbon (C_C) is coplanar with the three O atoms. In contrast, FEC^- is bent (Fig. 2d), with C_C now sp^3 hybridized. This leads to a large “reorganization energy” in the Marcus theory sense,³¹ discussed below. We define the C_C out-of-plane displacement R as the scalar product between (i) the normalized vector product connecting the three O-atoms, and (ii) $(\mathbf{R}_\text{C} - \mathbf{R}_{\text{Oave}})$,

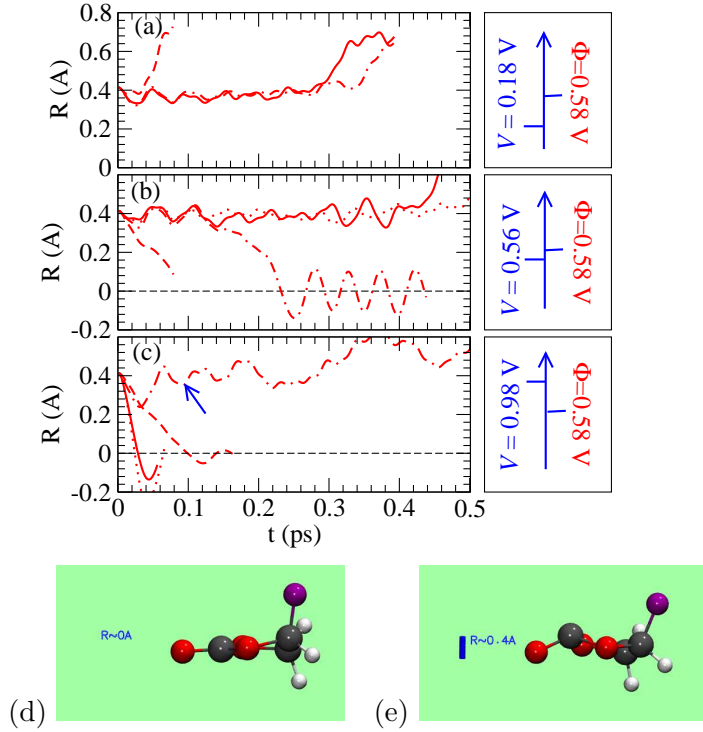


FIG. 2: (a)-(c) R as a function of time at various anode potentials \mathcal{V} . Different line shapes denote trajectories with different initial configurations. (d)&(e) Optimized FEC and FEC^- molecules. Out-of-plane coordinates R are illustrated. Purple circles represent F atoms.

where “Oave” is the mean position of the three oxygen atoms. $R=0.0$ Å and 0.4 Å in the optimized FEC and FEC^- geometries. Monitoring R grants easy access to FEC charge states. To initiate AIMD simulations, we first conduct MC using classical force fields (see the S.I.), then run AIMD for 1.0 ps while freezing all FEC^- atoms, and finally remove FEC constraints at “ $t=0$ ” of AIMD trajectories. The time evolution of R are shown in Fig. 2.

The reduction potential of FEC in bulk liquid regions is predicted to be $\Phi=0.58$ eV when it is not coordinated to Li^+ (S.I.). If $\mathcal{V}(\sigma = 0, n_{\text{Li}}) < \Phi$, the excess e^- should stay on FEC^- , ultimately leading to a second reduction of FEC^- and rapid decomposition.^{30,32} In the opposite case, the excess e^- should be transferred to the electrode. The S.I. shows that this expectation is always satisfied with different initial configurations on less electrochemically active basal plane surfaces. At edge planes, this test is successful, but less than 100 % of the time. When $\mathcal{V} \sim 0.18$ V ($n_{\text{Li}}=0.667$), lower than $\Phi=0.58$ V, FEC^- persists in all trials until it absorbs a second e^- and decomposes (Fig. 2a). This dovetails with our expectation.

When $\mathcal{V}=0.56$ V, very close to Φ , FEC^- is stable for hundreds of femtoseconds until it decomposes in two out of four trials; in the remaining two cases FEC^- loses its electron (Fig. 2b). Given our statistical uncertainties, this 50/50 split in the outcome is reasonable. When $\Phi < \mathcal{V}=0.98$ V, FEC^- should give up its excess e^- . This is observed 3 out of 4 times (Fig. 2c).

On the whole, Fig. 2 demonstrates that \mathcal{V} calibrated using Li^+ transfer also correctly governs e^- transfer. The one glaring “error” at $\mathcal{V}=0.98$ V is apparently due to overly rapid C-O bond breaking in FEC^- predicted using the PBE functional. This occurs within 100 fs (arrow in Fig. 2c; the predicted MP2 barriers for breaking this bond in EC^- and FEC^- are consistent with slower reaction rates.^{29,30}). Afterwards, the FEC^- ring cannot be reformed in AIMD timescale even if the anode potential favors it. It is also worth pointing out that DFT/PBE allows unphysical splitting of an excess e^- between the electrode and the redox center, artificially accelerating e^- transfer rate,³³ and may make Fig. 2 unduly sensitive to initial configurations. Instantaneous fluctuations in the potential experienced by redox centers are physical and real, but e^- transfer occurs over a finite timescale that partially averages out the fluctuations. Despite this, the overall trend of \mathcal{V} and Φ correspondence is correctly predicted: as \mathcal{V} decreases, FEC^- retains its excess e^- more readily.

C. Excess Electrons Form Localized States in the Gap

Figure 3 depicts spatially-demarcated DFT Kohn Sham spin-orbital levels at $t=0$ ps in two trajectories taken from Fig. 2b & c. In panel (a) ($\mathcal{V}=0.56$ V), the highest occupied molecular orbital (HOMO) is localized on FEC^- — reminiscent of a polaron in solid state physics — just below the Fermi level (E_F). FEC^- is found to decompose from this configuration. In panel (b), $V=0.98$ V, higher than $\Phi=0.58$ V; the localized orbital resides above E_F , and FEC^- loses its excess e^- rapidly in this trajectory. Fig. 3 illustrates that, for organic carbonate-based liquid electrolytes, the thermodynamic onset of electrolyte electrochemical reduction and SEI formation occurs when E_F coincides with the organic carbonate *localized* orbital found in the gap between liquid HOMO and liquid LUMO (lowest unoccupied molecular orbital or liquid conduction band minimum).³⁴ SEI formation does *not* begin, thermodynamically speaking, when the electrolyte LUMO coincides with the anode Fermi level, as has been widely assumed in the literature.²¹ The LUMO lies above the organic

carbonate localized orbital and exhibits substantial statistical fluctuations; however it may influence e^- transfer kinetics if electron transfers from the anode, through a substantial liquid layer, to FEC in the bulk liquid electrolyte region, instead of towards FEC that diffuses near the anode surface.

The above discussion adopts the solid state physics language often used in the battery community. It is important and of great interest to reconcile our study with molecular electrochemistry terminology³⁵ less often featured in battery studies. According to Marcus theory,³¹ e^- injection into FEC is accompanied with reorganization (free) energies (λ). For FEC^- , λ contains a large intramolecular component, and is not solely due to “outer shell” solvation effects. The “polaronic shift” of the HOMO of FEC^- , from above the liquid conduction band edge if FEC^- were flat, to within the liquid gap due to FEC^- geometry change and dielectric solvation, is a non-trivial manifestation of this λ . Quantitatively, the vertical electron affinity should be at a value λ above the molecular reduction potential Φ .³⁶ Unfortunately, it is difficult to compute λ in simulation cells with electrodes which are electron conductors. For example, the liquid electrolyte LUMO at frozen liquid geometry tend to reside above the Fermi level. As a result, injecting an e^- to the system to calculate the vertical electron affinity immediately populates the Fermi level of the electrode, not the the electrolyte, unless constrained DFT methods are used in the electrolyte region. In this sense, the systems considered in this work may differ from electrodes with a significant band gap, like TiO_2 .³⁷ Thus all AIMD simulations in this work report adiabatic free energy changes and redox potentials, not vertical excitations that include λ . To estimate λ , we have applied a localized basis set and dielectric continuum approach similar to Ref. 29. We find that the total λ for FEC is 3.2 eV. This is somewhat larger than that of the structurally similar EC.²⁹ Our predicted λ can be compared with future optical measurements in organic solvents analogous to those in aqueous media.³⁶ Incidentally, the wide separation between the localized excess e^- orbital in FEC^- and the liquid electrolyte HOMO minimizes hybridization between the localized state and solvent orbitals, which has been shown to be important for accurate DFT treatment of anions.^{36,38}

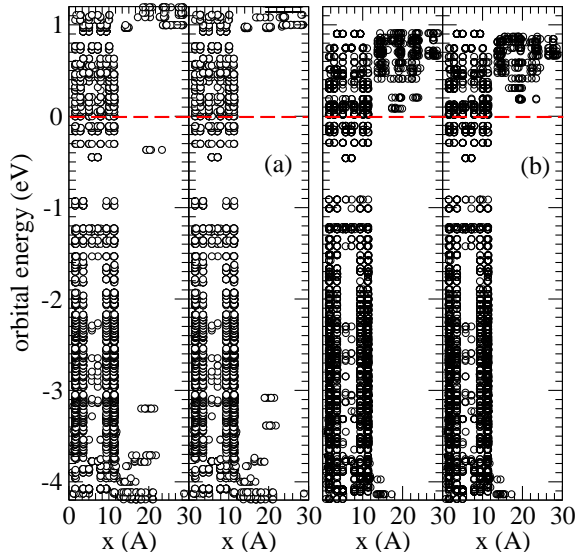


FIG. 3: Instantaneous Kohn-Sham orbital decomposed on to atoms at their x -coordinates at $t=0$ ps in Fig. 2b& c. $0 < x < 13.4$ Å denotes the metallic LiC_6 region; outside that range resides the liquid electrolyte which has a wide band gap. The Fermi level is at $E=0.0$ eV. Panels a & b depict the majority and minority spin channels of on trajectory each in Fig. 2a and Fig. 2b. The excess e^- “polaron” orbital of FEC resides in the majority spin channel, near E_F , in the electrolyte region.

D. PF_6^- Electrochemical Reduction

Finally, this potential-calibration technique is used to investigate possible PF_6^- reductive decomposition on anode surfaces as \mathcal{V} varies. A recent AIMD study has predicted rapid reductive decomposition of PF_6^- into LiF and PF_n^{q-} fragments, $n \leq 4$, at liquid EC/graphite edge interfaces.³⁹ Seemingly consistent with this prediction, simple cluster-based calculations suggests that the LiPF_6 “molecule” has a reduction potential of 1.46 V (S.I.), far above LiC_6 potentials during battery charging. However, such a PF_6^- reduction signature has not been observed in cyclic voltametry. Experimentally, the SEI formed in LiPF_6 -based electrolytes is known to contain LiF from PF_6^- breakdown, but it has been widely accepted that PF_6^- decomposes thermally or due to reaction with trace water over a period of hours,^{19,20} not electrochemically in seconds.

To reconcile these observations, we note that, unlike FEC reduction, e^- transfer to PF_6^- occurs in concert with P-F bond breaking. This is reminiscent of alkyl halide reduction,³⁵

which is clearly voltage dependent. Previous PF_6^- modeling work³⁹ has not specified its anode potential. In Fig. 4, we apply AIMD potential-of-mean-force ($\Delta W(R)$) techniques to estimate the free energy barrier (ΔG^*) of PF_6^- decomposition at two different potentials.

The trajectories include a PF_6^- pre-equilibrated at each graphite edge, charge-balanced by Li^+ in the electrolyte. The 3-atom reaction coordinate is $R' = |\mathbf{R}_P - \mathbf{R}_F| - |\mathbf{R}_{\text{Li}} - \mathbf{R}_F|$; P, F, and Li atoms are chosen such that they are in position to react at $t=0$ ps. Increasing R' is correlated with F^- transfer from P to an edge Li. Umbrella sampling potentials of the form $A(R' - R_o)^2/2$ are enforced, where $B=4$ to 10 eV and R_o span the range between the reactant and the transition state. See the S.I. for details.

Figure 4a shows that, at $\mathcal{V}=0.56$ V ($n_{\text{Li}}=0.583$), ΔG^* is at least 0.9 eV. As soon as one P-F bond breaks completely, e^- is transferred, other F^- 's detach from the P-atom spontaneously (Fig. 4d), and these irreversible steps render a quasi-equilibrium sampling of $\Delta W(R)$ in the barrier top region impossible. In contrast, at $\mathcal{V}=-0.21$ V ($n_{\text{Li}}=0.75$), the barrier appears not much higher than 0.2 eV. Fig. 4 indicates that PF_6^- electrochemical reduction may occur during the initial stage of SEI formation if the anode is at sufficiently low potentials, although this process faces competition from solvent reductive decomposition.

Conclusions

In conclusion, we have calibrated the anode potential ($\mathcal{V}(\sigma = 0, n_{\text{Li}})$) of lithium intercalated graphite edge planes at zero surface electronic charge ($\sigma=0$) as a function of the edge Li content (n_{Li}) by computing the free energy of Li^+ transfer between electrode and liquid electrolyte. The estimated \mathcal{V} is shown to be reasonable by correlating with observed electron transfer from reduced fluoroethylene carbonate (FEC^-) radical anions inserted into the liquid region. Electrochemical reduction of PF_6^- at the pristine edge plane is shown to be viable at low potentials and to exhibit potential-dependent kinetics. This reduction pathway may need to be considered during SEI formation, in addition to thermal/impurity water-induced PF_6^- decomposition routes widely accepted in the literature. In the future, optimization of the free energy with respect to all surface parameters (N_{Li} and σ) will be performed, and our method will be used to study the dynamics of Li^+ insertion into passivated anodes as a function of the applied potential.

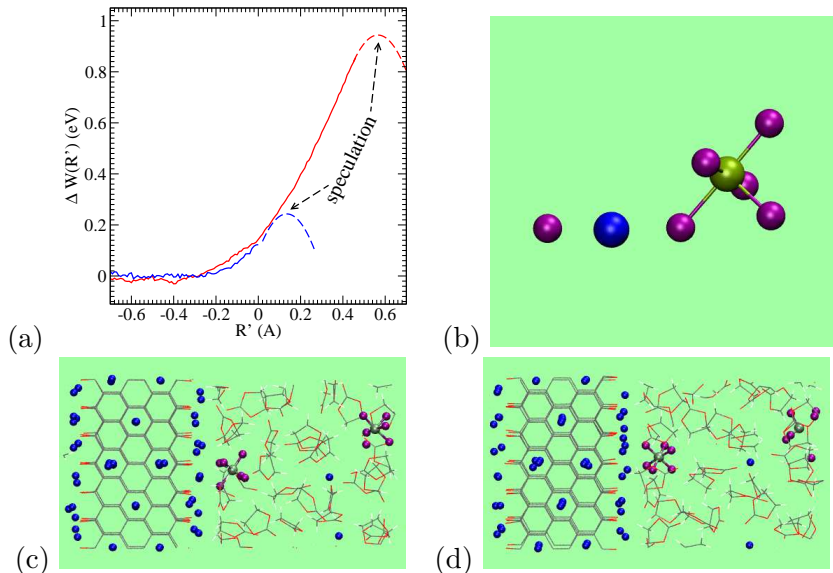


FIG. 4: (a) Potentials-of-mean-force (PMF) of PF_6 electrochemical decomposition, as functions R' at estimated 0.56 V (red, $n_{\text{Li}}=0.583$) and -0.21 V (blue, $n_{\text{Li}}=0.750$), respectively. The solid line portions depict actual data. The barriers must reside in the dashed line regions because PMF calculations there lead to spontaneous PF_6^- decomposition in picosecond timescale. (b) Reduced $\text{Li}^+:\text{F}^-:\text{PF}_5^-$ fragment from static, localized basis-set calculations. (c)& (d): AIMD snapshots in PMF trajectories at $V=0.56$ V, $R' \sim -0.21$ and $R' \sim +0.5\text{\AA}$, respectively. The rightmost PF_6^- has decomposed in panel (d); recall that periodic boundary conditions are used.

Acknowledgement

We thank Kevin Zavadil and Jun Cheng for interesting discussions. This work was supported by Nanostructures for Electrical Energy Storage (NEES), an Energy Frontier Research Center funded by the U.S. Department of Energy, Office of Science, Office of Basic Energy Sciences under Award Number DESC0001160. Sandia National Laboratories is a multiprogram laboratory managed and operated by Sandia Corporation, a wholly owned subsidiary of Lockheed Martin Corporation, for the U.S. Department of Energy's National Nuclear Security Administration under contract DE-AC04-94AL85000.

† Electronic supporting Information available. See DOI:TBA.

- ¹ K. Xu, *Chem. Rev.*, 2004, **104**, 4303-4417.
- ² P. Verma, P. Maire and P. Novak, *Electrochim. Acta*, 2010, **55**, 6332-6341.
- ³ Y.S. Jung, A.S. Cavanagh, A.C. Dillon, M.D. Groner, S.M. George, and S.-H. Lee, *J. Electrochem. Soc.* 2010, **157**, A75.
- ⁴ Y. Yamada, K. Furukawa, K. Sodeyama, K. Kikuchi, M. Yaegashi, Y. Tateyama and A. Yamada, *J. Am. Chem. Soc.*, 2014, **136**, 5039-5046.
- ⁵ M.K.Y. Chan, C. Wolveton, and J.P. Greeley, *J. Am. Chem. Soc.*, 2012, **134**, 14362-14374.
- ⁶ V.S. Bryantsev and M. Blanco, *J. Phys. Chem. Lett.*, 2011, **2**, 379-383.
- ⁷ J. Chen, Y.F. Li, P. Sit and A. Selloni, *J. Am. Chem. Soc.*, 2013, **135**, 18774-18777.
- ⁸ J. Cheng and M. Sprik, *Phys. Chem. Chem. Phys.*, 2012, *14*, 11245-11267.
- ⁹ M. Otani, I. Hamada, O. Sugino, Y. Morikawa, Y. Okamoto and T. Ikeshoji, *J. Phys. Soc. Jpn.*, 2008, **77**, 024802.
- ¹⁰ R. Jinnouchi, K. Kodama, T. Hatanaka and Y. Morimoto, *J. Electroanal. Chem.*, 2014, **716**, 31-44.
- ¹¹ M.E. Bjorketun, Z.H. Zeng, R. Ahmed, V. Tripkovic, K.S. Thygesen and J. Rossmeisl, *Chem. Phys. Lett.*, 2013, **555**, 145-148.
- ¹² S. Schnur and A. Gross, *Catalysis Today*, 2011, **165**, 129-137.
- ¹³ L.M.C. Pinto, E. Spohr, P. Quaino, E. Santos, and W. Schmickler, *Angewandte Chemie Int. Ed.*, 2013, **52**, 7883-7885.
- ¹⁴ C.J. Barile, R. Spatney, K.R. Zavadil, and A.A. Gewirth, *J. Phys. Chem. C*, 2014, **118**, 10694-10699.
- ¹⁵ K. Leung and C.M. Tenney, *J. Phys. Chem. C*, 2013, **117**, 24224-24235.
- ¹⁶ See, e.g., J. Vatamanu, O. Borodin and G.D. Smith, *J. Phys. Chem. C* 2012, **116**, 1114-1121, and references therein.
- ¹⁷ J.D. Foster, S.J. Harris and J.J. Urban, *J. Phys. Chem. Lett.* 2014, **4**, 2007-2011.
- ¹⁸ L.R. Pratt, *J. Phys. Chem.*, 1992, **96**, 25-33.
- ¹⁹ S.F. Lux, L.T. Lucas, E. Pollak, S. Passerini, M. Winter, R. Kostecki, *Electrochem. Commun.*, 2012, **14**, 47-50.

- ²⁰ A.V. Plakhotnyk, L. Ernst and R. Schmutzler, *J. Fluorine Chemistry*, 2005, **126**, 27-31.
- ²¹ In the literature, the onset of SEI formation is often assumed to occur when the LUMO aligns with E_F in all electrolytes. See, e.g., J.B. Goodenough and K.-S. Park, *J. Am. Chem. Soc.*, 2013, **135**, 1167-1176.
- ²² K. Leung and J.L. Budzien, *Phys. Chem. Chem. Phys.*, 2010, **12**, 6583-6586.
- ²³ Edge C atoms are terminated in various functional groups. See R.L. McCreery, *Chem. Rev.*, 2008, **108**, 2646-2687.
- ²⁴ G. Kresse and J. Furthmüller, *Phys. Rev. B*, 1996, **54**, 11169.
- ²⁵ G. Kresse and J. Joubert, *Phys. Rev. B*, 1999, **59**, 1758-1775.
- ²⁶ J.P. Perdew, K. Burke and M. Ernzerhof, *Phys. Rev. Lett.*, 1996, **77**, 3865-3868.
- ²⁷ We have used LiC_6 inside the electrode throughout, instead of pure graphite at high voltage and LiC_6 at low. The rationale is that the electrolyte does not see the electrode interior. See Ref. 22 for a discussion.
- ²⁸ P.C. Rusu and G. Brocks, *J. Phys. Chem. B*, 2006, **110**, 22628-22634.
- ²⁹ K. Leung, *Chem. Phys. Lett.*, 2013, **568-569**, 1-8.
- ³⁰ K. Leung, S.B. Rempe, M.E. Foster, Y. Ma, J.M. Martinez de Hoz, N. Sai and P.B. Balbuena, *J. Electrochem. Soc.*, 2014, **161**, A213-A221, and references therein.
- ³¹ R.A. Marcus, *Rev. Mod. Phys.*, 1993, **65**, 599.
- ³² Organic carbonates have been shown to exhibit higher second reduction potentials than first in high dielectric media, especially if they have broken bonds.²⁹
- ³³ P. Mori-Sánchez, A.J. Cohen and W. Yang, *Phys. Rev. Lett.*, 2008, **100**, 146401.
- ³⁴ Although Kohn-Sham orbitals are not physical quantities in general and the above discussion is therefore qualitative, at the onset of FEC reduction, when the occupied FEC^- HOMO orbital is at the Fermi level, the change of total electronic energy as a function of the partial occupancy of this orbital should indeed correspond to the orbital energy. In that sense Fig. 3 is well defined at the onset of FEC reduction.
- ³⁵ See, e.g., J.-M. Saéant, *Chem. Rev.* 2008, **108**, 2348-2378.
- ³⁶ C. Adriaanse, J. Cheng, V. Chau, M. Sulpizi, J. VandeVondele and M. Sprik, *J. Phys. Chem. Lett.*, 2012, **3**, 3411-3415.
- ³⁷ J. Cheng, J. VandeVondele and M. Sprik, *J. Phys. Chem. C* 2014, **118**, 5437.
- ³⁸ D. Opalka, T.A. Pham, M. Sprik, and G. Galli, *J. Chem. Phys.*, 2014, **141**, 034501.

³⁹ P. Ganesh, P.R.C. Kent and D. Jiang, *J. Phys. Chem. C*, 2012, **116**, 24476-24481.